JOURNAL OF GEOPHYSICAL RESEARCH: ATMOSPHERES, VOL. 118, 11,807–11,823, doi:10.1002/2013JD019760, 2013

Comparison of CH_4 inversions based on 15 months of GOSAT and SCIAMACHY observations

Guillaume Monteil,[1,2] Sander Houweling,[2,1] André Butz,[3] Sandrine Guerlet,[2,4] Dinand Schepers,[2] Otto Hasekamp,[2] Christian Frankenberg,[5] Remco Scheepmaker,[2] Ilse Aben,[2] and Thomas Röckmann[1]

Received 7 March 2013; revised 27 September 2013; accepted 1 October 2013; published 17 October 2013.

[1] Over the past decade the development of Scanning Imaging Absorption Spectrometer for Atmospheric Chartography (SCIAMACHY) retrievals has increased the interest in the use of satellite measurements for studying the global sources and sinks of methane. Meanwhile, measurements are becoming available from the more advanced Greenhouse Gases Observing Satellite (GOSAT). The aim of this study is to investigate the application of GOSAT retrievals to inverse modeling, for which we make use of the TM5-4DVAR inverse modeling framework. Inverse modeling calculations are performed using data from two different retrieval approaches: a full physics and a lightpath proxy ratio method. The performance of these inversions is analyzed in comparison with inversions using SCIAMACHY retrievals and measurements from the National Oceanic and Atmospheric Administration-Earth System Research Laboratory flask-sampling network. In addition, we compare the inversion results against independent surface, aircraft, and total-column measurements. Inversions with GOSAT data show good agreement with surface measurements, whereas for SCIAMACHY a similar performance can only be achieved after significant bias corrections. Some inconsistencies between surface and total-column methane remain in the Southern Hemisphere. However, comparisons with measurements from the Total Column Carbon Observing Network in situ Fourier transform spectrometer network indicate that those may be caused by systematic model errors rather than by shortcomings in the GOSAT retrievals. The global patterns of methane emissions derived from SCIAMACHY (with bias correction) and GOSAT retrievals are in remarkable agreement and allow an increased resolution of tropical emissions. The satellite inversions increase tropical methane emission by 30 to 60 Tg CH_4/yr compared to initial a priori estimates, partly counterbalanced by reductions in emissions at midlatitudes to high latitudes.

Citation: Monteil, G., S. Houweling, A. Butz, S. Guerlet, D. Schepers, O. Hasekamp, C. Frankenberg, R. Scheepmaker, I. Aben, and T. Röckmann (2013), Comparison of CH_4 inversions based on 15 months of GOSAT and SCIAMACHY observations, *J. Geophys. Res. Atmos.*, *118*, 11,807–11,823, doi:10.1002/2013JD019760.

1. Introduction

[2] Methane is the second most important anthropogenic greenhouse gas. Its concentration in the atmosphere has grown by a factor 2.5 since the preindustrial period, and it is currently responsible for approximately 20% of the anthropogenic greenhouse effect [*Denman et al.*, 2007]. It has been proposed as an "easy target" for global warming mitigation policies [*Hansen et al.*, 2000; *Shindell et al.*, 2012] because of its high global warming potential [*Forster et al.*, 2007] and because of its short atmospheric lifetime compared with CO_2 [*Dentener et al.*, 2003]. The technical mitigation potential of CH_4 (amount of methane emissions that could be reduced by technological efficiency improvements) has been estimated at about half of the projected anthropogenic emissions in 2030 [*Höglund-Isaksson*, 2012].

[3] Predicting the future atmospheric methane concentration requires a thorough understanding of the processes controlling it. Anthropogenic emissions (mainly from agriculture, waste management, and fossil fuel production) are the main drivers of the increase over the last century. However, natural sources (wetlands, termites, geological activity)

[1]Institute of Marine and Atmospheric Research Utrecht, Utrecht University, Utrecht, The Netherlands.
[2]SRON Netherlands Institute for Space Research, Utrecht, The Netherlands.
[3]IMK-ASF, Karlsruhe Institute of Technology, Eggenstein-Leopoldshafen, Germany.
[4]Now at Laboratoire de Météorologie Dynamique, Institut Pierre-Simon Laplace, Paris, France.
[5]Jet Propulsion Laboratory, California Institute of Technology, Pasadena, USA.

Corresponding author: G. Monteil, Institute of Marine and Atmospheric Research Utrecht, Utrecht University, 3584CC Utrecht, The Netherlands. (g.monteil@sron.nl)

2169-897X/13/10.1002/2013JD019760

and sinks (mainly oxidation of methane by the hydroxyl radical, OH) also have sensitivity to climate change.

[4] Large-scale methane surface fluxes are not directly measurable. However, inverse modeling techniques can be used to derive information on these fluxes from observations of atmospheric methane concentrations. Inverse modeling techniques usually combine observations of methane mixing ratios with a priori knowledge on methane emissions to obtain a statistical best estimate of these emissions [*Mikaloff Fletcher et al.*, 2004; *Bousquet et al.*, 2006; *Meirink et al.*, 2008b]. The quality of the estimate is highly dependent, among other factors, on the availability and quality of measurements.

[5] Since the methane lifetime in the atmosphere is long (∼9 years) [*Dentener et al.*, 2003] compared to the typical time scales of long-range transport (∼1 year for interhemispheric air exchange), global networks of surface concentration measurements (such as the National Oceanic and Atmospheric Administration-Earth System Research Laboratory (NOAA/ESRL), Advanced Global Atmospheric Gases Experiment, and Commonwealth Scientific and Industrial Research Organisation networks [*Dlugokencky et al.*, 2013; *Rigby et al.*, 2008; *Francey et al.*, 1999]) provide a good representation of large-scale variations of methane concentrations such as the interhemispheric gradient and seasonal and interannual variability. From this information, important constraints can be derived about variations in the imbalance of global-scale methane sources and sinks [*Crutzen et al.*, 1997; *Dlugokencky et al.*, 2003; *Wang et al.*, 2004; *Bousquet et al.*, 2010]. Unfortunately, due to the sparseness and the uneven distribution of these surface networks, they provide accurate regional constraints only in a few densely monitored regions (mostly North America and Europe). This means that potentially large methane emissions from tropical regions are poorly constrained. For this reason, inverse modeling constrained only by global surface monitoring networks is mainly used for studying the methane budgets and interannual variations integrated over large regions [*Crutzen et al.*, 1997; *Bousquet et al.*, 2006, 2010]. Another application is regional-scale inverse modeling using measurement from tall towers, in regions where a tall tower network exists, such as the Integrated Carbon Observation System network in Europe [*Villani et al.*, 2010].

[6] In contrast, satellite observations of methane provide a more extensive and homogeneous coverage than in situ networks. Since they quantify a column-mixing ratio, and not only a local one like surface measurements, they provide a constraint on a larger fraction of the atmosphere than surface observations. Depending on the sensitivity of the instrument and on the retrieval technique, they may be sensitive to the upper troposphere/lower stratosphere area. This is considered an advantage since it should lead to a more complete representation of the atmosphere, but it also makes inversions using satellite retrievals more sensitive to model errors in the upper troposphere and stratosphere. Important drawbacks of satellite retrievals are that they are available only for a limited range of atmospheric conditions (absence of clouds, low aerosol load) and that they are less accurate and more difficult to validate than in situ measurements.

[7] In the past 15 years, several satellite instruments have been launched for measuring methane in the troposphere. Of particular importance for inverse modeling are SCIAMACHY (Scanning Imaging Absorption Spectrometer for Atmospheric Chartography, onboard ENVISAT), which has been in orbit since March 2002 but stopped transmitting data in April 2012, and Tanso-FTS (Thermal and Near Infrared Sensor for Carbon Observation), aboard the Greenhouse gases observing satellite (GOSAT), which was launched in January 2009. Both SCIAMACHY and GOSAT measure CH_4 exploiting its shortwave-infrared absorption in the solar spectrum. They are therefore sensitive to methane in the whole troposphere, which makes them particularly suitable for inverse modeling of surface emissions. Several other instruments (TES [*Wecht et al.*, 2012], IASI [*Razavi et al.*, 2009], and AIRS [*Xiong et al.*, 2008]) are measuring methane in the thermal infrared (TIR), but with a peak sensitivity near the tropopause, and are hence better suited for studying large-scale transport of methane [*Crevoisier et al.*, 2009; *Xiong et al.*, 2010; *Wecht et al.*, 2012].

[8] Several XCH_4 (column-averaged dry mole fraction of CH_4) retrievals using SCIAMACHY observations have been published [*Frankenberg et al.*, 2005b; *Buchwitz et al.*, 2005; *Schneising et al.*, 2009]. Early versions of the SCIAMACHY IMAP (iterative maximum a posteriori) retrieval [*Frankenberg et al.*, 2005a] pointed to significantly higher tropical emissions than accounted for in emission inventories, supporting the hypothesis of aerobic methane emissions from living plants [*Keppler et al.*, 2006]. Further development of the SCIAMACHY IMAP XCH_4 retrieval showed that part of the strong methane signal in the tropics was caused by spectroscopic uncertainties [*Frankenberg et al.*, 2008, 2011]. Aerobic CH_4 emissions from living plants were found to be far lower than initially suggested [*Dueck et al.*, 2007; *Nisbet et al.*, 2009; *Keppler et al.*, 2009; *Vigano*, 2010; *Querino et al.*, 2011] and may be insignificant for the global budget. Recent inversions using SCIAMACHY still show a disagreement between tropical bottom-up methane emissions inventories and emission estimates derived from satellite observations [*Bergamaschi et al.*, 2009], which points to remaining uncertainties in tropical methane emissions, most likely related to underestimated wetland emissions.

[9] GOSAT XCH_4 retrievals have been published by several groups [*Parker et al.*, 2011; *Yoshida et al.*, 2011; *Butz et al.*, 2011]. In this study we make use of the *RemoTeC* GOSAT XCH_4 retrievals which are available using two different techniques: The Proxy retrieval [*Butz et al.*, 2011; *Schepers et al.*, 2012] which was originally developed for SCIAMACHY [*Frankenberg et al.*, 2005a] and the recently developed Full Physics approach [*Butz et al.*, 2010; *Schepers et al.*, 2012], which is a combined retrieval of CH_4, CO_2, and aerosol parameters. Extensive comparisons between these GOSAT retrievals and ground-based total-column CH_4 measurements from TCCON (Total Column Carbon Observing Network) [*Wunch et al.*, 2010] pointed to significant improvements in accuracy and precision compared with SCIAMACHY [*Butz et al.*, 2011]. On the other hand, the long integration time of the Tanso-FTS instrument onboard GOSAT leads to a reduction in sampling frequency. This reduces the measurement coverage by roughly an order of magnitude compared with SCIAMACHY. *Fraser et al.* [2012] published inverse modeling simulations constrained by GOSAT-Proxy retrievals from *Parker et al.* [2011], but

it is the first time a Full Physics retrieval is being used in an inversion.

[10] The goal of this paper is to investigate the use of the new *RemoTeC* XCH_4 retrievals for estimating global methane emissions using atmospheric inverse modeling. Inversions are performed using the two GOSAT retrieval methods on a 15 month period (from May 2009 to August 2010), and results are compared to inversions using (1) surface concentration measurements only and (2) SCIAMACHY retrievals and surface concentration measurements. The aim is to verify whether the emission adjustments using GOSAT confirm earlier reported findings using SCIAMACHY and whether the improved GOSAT measurement quality provides additional constraints on CH_4 fluxes.

[11] This intercomparison is a first step toward the combined use of SCIAMACHY and GOSAT retrievals in methane inversions spanning a longer time period. This addresses the problem of the limited lifetime of satellite instruments and the need to combine instrumental records for conducting long-term studies, which is relevant also in the context of new satellites that are planned for launch the coming years (OCO-2, TROPOMI on Sentinel-5 precursor, CarbonSat, and GOSAT-2). Identifying strengths and shortcomings of SCIAMACHY and GOSAT from an atmospheric modeling perspective may help improve the specification and design of new instruments.

[12] In section 2 we describe our model and its initial setup and the main characteristics of the observational data sets used. In section 3 we first verify that each inversion is able to reproduce methane observations from different data sets. Then we present and discuss the emissions obtained using different inverse modeling setups, focusing on the role of the systematic and random components of measurement uncertainty, and measurement coverage. Finally, we discuss the role of other remaining sources of uncertainty.

2. Methods

2.1. Model

[13] In this study we use the TM5-4DVAR inverse model described in *Meirink et al.* [2008a]. TM5 is a chemistry transport model for calculating the spatiotemporal distribution of atmospheric tracers given surface fluxes, atmospheric chemistry, and transport. Model simulations are carried out at a horizontal resolution of 6° × 4° (longitude × latitude) and 25 hybrid sigma-pressure levels in the vertical. Transport is driven by meteorological fields from the European Centre for Medium-Range Weather Forecasts (ECMWF) ERA-interim reanalysis project [*Dee et al.*, 2011]. The most important update since the TM5 model version described in *Meirink et al.* [2008a] is the parametrization of horizontal diffusion, described in section 2.1. The 4DVAR is a data-assimilation method originally developed for numerical weather prediction but now widely used for studying atmospheric chemical composition [*Talagrand and Courtier*, 1987; *Fisher and Lary*, 1995]. It minimizes the cost function

$$J(\mathbf{x}) = \underbrace{\frac{1}{2}(\mathbf{x}-\mathbf{x_b})^T\mathbf{B}^{-1}(\mathbf{x}-\mathbf{x_b})}_{J_b} + \underbrace{\frac{1}{2}(\mathbf{y}-\mathbf{Hx})^T\mathbf{R}^{-1}(\mathbf{y}-\mathbf{Hx})}_{J_{\mathrm{obs}}}, \quad (1)$$

where the state vector $\mathbf{x}$ is the set of parameters that we seek to optimize, $\mathbf{x_b}$ is the a priori knowledge of $\mathbf{x}$, and $\mathbf{y}$ is a vector of observations. $\mathbf{Hx}$ represents model estimates for observations corresponding to $\mathbf{y}$. $\mathbf{B}$ and $\mathbf{R}$ are, respectively, the error covariance matrices of the a priori fluxes and of the observations. The 4DVAR algorithm minimizes the cost function iteratively. For an initial state vector $\mathbf{x} = \mathbf{x_b}$, the local cost function gradient $\nabla J(\mathbf{x})$ is calculated using the adjoint method [*Errico*, 1997] and is used to determine an updated state vector that leads to a lower value of $J(\mathbf{x})$ (using the conjugate gradient algorithm [*Lanczos*, 1950]). This process is repeated until the gradient norm decreases below a preset convergence condition. Details about the implementation in TM5 can be found in *Meirink et al.* [2008a] and references therein.

[14] 4DVAR was first implemented in TM5 by *Meirink et al.* [2008b] to optimize methane emissions and was further developed by *Bergamaschi et al.* [2009] and applied to other tracers [*Hooghiemstra et al.*, 2011, 2012; *Montzka et al.*, 2011; *Basu et al.*, 2013].

[15] The state vector $\mathbf{x}$ is composed of the monthly emissions into each surface grid box of the model and the a priori methane concentration field on the first day of the simulation. Monthly emission uncertainties (diagonal terms of $\mathbf{B}$ in equation (1)) are set as 50% of the a priori fluxes in each grid box. Emission error correlations (off-diagonal terms of $\mathbf{B}$) are modeled using a Gaussian function of the distance between grid cells (both in time and space), using spatial and temporal correlation lengths of, respectively, 500 km and 1 month. A similar 500 km horizontal correlation length is used for the a priori CH_4 concentration field, in combination with a vertical correlation determined using the National Meteorological Center (NMC) method [*Parrish and Derber*, 1992; *Meirink et al.*, 2006].

[16] The treatment of observations and observational errors ($\mathbf{y}$ and $\mathbf{R}$) and the calculation of model-to-observation distances ($\mathbf{y} - \mathbf{Hx}$) are described in section 2.3.3.

[17] In our simulations the TM5 model has been extended with a horizontal diffusion parameterization, following results of *Patra et al.* [2011] showing that TM5 underestimates the interhemispheric mixing in comparison with other models and SF6 measurements. The new parameterization is an extension of the scheme by *Prather et al.* [1987], which accounts for horizontal mixing in presence of deep convection. Large convection cells are common along the Intertropical Convergence Zone (ITCZ), which explains why explicit representation of horizontal diffusion effectively enhances interhemispheric mixing. The original scheme has been modified such that the diffusion coefficients are scaled to the sum of the convective entrainment and detrainment fluxes that are used for convection in the model. As a criterion for "deep convection" we use the difference between cloud top and cloud base, which should exceed 500 hPa. Like in *Prather et al.* [1987], a global scaling factor is used to bring the simulated north-south gradient of SF6 in agreement with measurements. Figure 1 shows the impact of the horizontal diffusion scheme on the TM5 simulated SF6 gradient using emissions as specified in the TRANSCOM-CH4 protocol [*Patra et al.*, 2011].

2.2. A Priori Sources and Sinks

[18] The model is forced by monthly emissions on a 6° × 4° grid. Except for biomass burning, all anthropogenic emissions are derived from emission maps of the EDGAR4.1

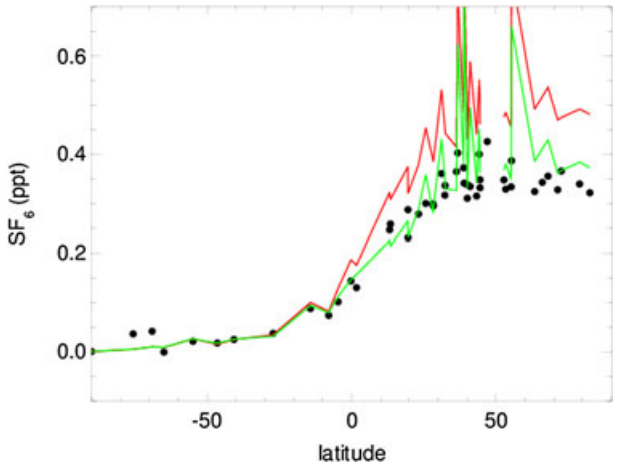

Figure 1. Comparison of model-simulated and observed latitudinal gradients of SF6. Concentrations are shown relative to NOAA site South Pole. Black: measurements (NOAA); green/red: TM5 with/without horizontal diffusion (models are evaluated at measurement locations (in time and space) for the year 2004).

inventory (http://edgar.jrc.ec.europa.eu) emission maps for 2005, corrected by scaling factors to account for the emission changes since 2005. For energy-production-related emission maps (such as coal mining and oil and gas production), the scaling factors are derived from annual energy statistics made available by British Petroleum (BP) (statistical review of world energy 2011, http://www.bp.com). To update emissions from agricultural sources (rice cultivation, cattle farming), we make use of Food and Agriculture Organization statistics (http://faostat.fao.org). For remaining anthropogenic emissions (such as waste treatment), a scaling factor was derived from the average 2000–2005 growth rate in the EDGAR4.1 database.

[19] EDGAR4.1 emission maps are annual. However, since rice emissions have important seasonal variations, we distributed them monthly according to the rice cropping calendar of *Matthews and Fung* [1987]. Other EDGAR sources were kept constant through the year.

[20] Monthly maps of biomass burning emissions are taken from the GFED3.1 inventory, except for those of agricultural waste burning that are taken from EDGAR4.1. Since it does not cover the year 2010, the 2009 emission map was reused in 2010.

[21] For natural wetland emission estimates, we used an average of the emissions calculated for the period 2003–2008 by *Spahni et al.* [2011] with the process-based model LPJ-WhyMe. LPJ-WhyMe accounts for emissions from wet soils as well as from methane oxidation under dry conditions (methane soil sink). Since LPJ-WhyMe also covers regions with intensive rice cultivation, these regions were not used, to avoid double counting with EDGAR4.1.

[22] Recent estimates of geological emissions of methane (from mud volcanoes and methane hydrates) point to a global source of 40 to 60 Tg CH_4/yr [*Etiope and Milkov*, 2004; *Kvenvolden and Rogers*, 2005; *Etiope et al.*, 2008]. However, despite considerable efforts to make an inventory of geological sources [*Etiope and Klusman*, 2002; *Bange et al.*, 2009; *Shakhova et al.*, 2010], the available estimates are based on measurements from a relatively small number of sites, and no comprehensive map of geologic emissions is yet available. For terrestrial geologic emissions, we accounted only for emissions reported in the Global On-Shore Gas and Oil Seeps (GLOGOS) database (http://www.searchanddiscovery.com/documents/2009/090806etiope/). The total emission was distributed evenly over reported sites for lack of quantitative information about the majority of sites. For oceanic seepages, a conservative estimate of 17 Tg CH_4/yr was distributed uniformly over the continental shelves.

[23] Tropospheric oxidation of methane by OH is calculated using monthly distribution of OH by *Spivakovsky et al.* [2000], adjusted by a single scaling factor (0.92) derived from inverse modeling of methyl chloroform in TM5 [*Montzka et al.* [2011]; M. Krol, personal communication]. The same OH field was used in 2009 and 2010. Stratospheric CH_4 lifetimes are derived from the Cambridge 2-D model [*Law and Pyle*, 1993; *Velders*, 1995] and account for CH_4 oxidation by OH, $O(^1D)$, and Cl radicals.

[24] A summary of the a priori methane emissions per source category is provided in Table 1.

2.3. Observations

[25] We used observational constraints from surface concentration measurements and from the GOSAT and SCIAMACHY satellite instruments. In this section we describe the observation data sets and the preprocessing that we applied to them.

2.3.1. Surface Concentration Measurements

[26] Measurement time series from 46 sites of the NOAA/ESRL cooperative flask-sampling network [*Dlugokencky et al.*, 2013] were used to constrain our inversions. The purpose of using these observations is to provide a reliable background constraint on CH_4 emissions. Therefore, only sites that provide good coverage during our inversion time period were selected. A map of selected sites is shown in Figure 2.

2.3.2. Satellite Observations

[27] Three retrieval data sets have been used in our inversions: the SCIAMACHY IMAPv5.5 retrieval [*Frankenberg et al.*, 2008, 2011] and the GOSAT RemoTeCv1.0 Proxy [*Schepers et al.*, 2012] and Full Physics retrievals [*Butz et al.*, 2010, 2011].

Table 1. A Priori Sources Strength for 2009 and 2010

Category	2009	2010
Biomass burning[a]	23.6	23.7
Wetlands	124.9	124.9
Geologic sources[b]	24.5	24.5
Rice cultivation	35.7	35.8
Agriculture[c]	110.6	110.6
Fossil sources[d]	118.8	125.0
Waste management[e]	61.1	62.4
Other anthropogenic	24.4	25.0
Other natural[f]	12.8	12.8
Total	536	545

[a]GFED3.1 biomass burning emissions and EDGAR4.1 agricultural waste burning.
[b]Marine and anthropogenic sources.
[c]Cattle and manure management.
[d]Coal mining and oil and gas production and distribution.
[e]Landfills and wastewater management.
[f]Termites and wild animals.

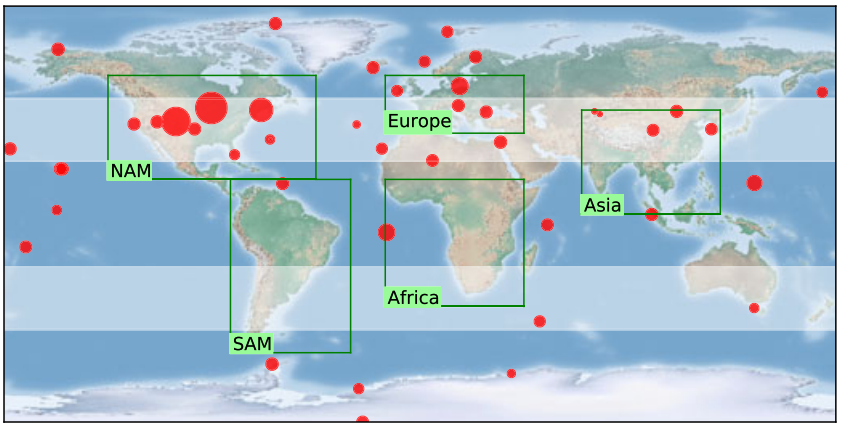

Figure 2. Location of surface measurements used in the inversions (red dots). The dot sizes are proportional to the number of measurements at each location. Definition of regions (green squares) and definition of zonal bands (shaded bands; from north to south: NPOL, NHET, TROP, and SHET) used in sections 3 and 4.

[28] All retrievals make use of measurements of the spectral radiance of Earth-reflected sunlight in the 1.65 μm absorption band of methane. In addition, information on the light path is needed to transform observed methane number densities into dry air mixing ratios. This requires an estimate of the integrated air mass that is sampled along the optical path.

[29] 1. In the Proxy method the total column of CO_2 (retrieved from its absorption band at 1.57 μm for SCIAMACHY and 1.6 μm for GOSAT) is taken as proxy of the sampled air mass, represented as

$$XCH_4 = \frac{[CH_4]_{obs}}{[CO_2]_{obs}} \times XCO_{2_{mod}}, \quad (2)$$

where $XCO_{2_{mod}}$ is a model-derived estimate of XCO_2, for which we use CarbonTracker 2009 [*Peters et al.*, 2007, 2010]. The method was first introduced for XCH_4 retrievals from SCIAMACHY but is also applied to GOSAT [*Schepers et al.*, 2012]. The strength of the proxy approach lies in the fact that perturbations in the optical path due to aerosol scattering efficiently cancel out in the $\frac{CH_{4_{obs}}}{CO_{2_{obs}}}$ ratio. This is based on the assumption that the utilized CH_4 and CO_2 absorptions bands are at a sufficiently small spectral distance from each other for the aerosol scattering properties and surface albedo to be similar. The method is also attractive from a computational point of view, since there is no need to account for scattering in the radiative transfer model. The main disadvantage is that the proxy XCH_4 retrievals rely on the quality of $CO_{2_{model}}$ and can therefore not be considered a fully independent measurement of XCH_4.

[30] 2. In the Full Physics retrieval approach, the information on scattering that is required for estimating the sampled air mass is retrieved from the measured spectra along with XCH_4 [*Butz et al.*, 2011]. The main advantage of this method compared with the proxy method is that it does not require a model-derived CO_2 field. On the other hand, the Full Physics approach can only account for scattering to a limited extend [*Schepers et al.*, 2012]. In addition, the method is less tolerant to cloud cover than the proxy method, which calls for a more stringent cloud filtering. These requirements on filtering for clouds and aerosols reduce the number of useful measurements for the full physics approach to 31% of the proxy approach.

[31] An estimate of retrieval uncertainty is calculated by the retrieval algorithms (by propagation of the instrumental and a priori retrieval parameters uncertainties). These uncertainties are on average 8.4 ppb for the GOSAT-Proxy retrievals and 9.9 ppb for the GOSAT-Full Physics. However, comparisons with independent data from the TCCON network [*Wunch et al.*, 2010] point to overall measurement uncertainties that are on average a factor 1.5–2 larger than the retrieval-derived uncertainty [*Butz et al.*, 2011; *Schepers et al.*, 2012]. In our simulations (and in Figure 3), we therefore scale the GOSAT retrievals uncertainties by a factor 1.5. For SCIAMACHY the retrieval uncertainty is higher, on average 27 ppb.

[32] Extensive data filtering is carried out to exclude measurements under various conditions which compromise the retrieval quality, cloud cover being the most limiting. The data filtering is specific to each instrument and each retrieval method.

[33] GOSAT-Full Physics retrievals are filtered according to the parameters described in *Butz et al.* [2011, auxiliary material]. Additionally, we filter out sunglint measurements (oceans) and Gain-M measurements (measurements using a different sensor configuration, used for high surface albedo situations). The filtering criteria for the GOSAT-Proxy retrieval differ from those of the Full Physics retrieval by more relaxed cloud-cover conditions (95% cloud-free instead of 99% for the Full Physics retrieval) and by the absence of scattering-based filtering conditions. For SCIAMACHY, we used the standard filtering settings of the IMAP retrieval (http://www.sciamachy.org/products/CH4/CH4vc_SRON_PSD_v5.pdf). Additionally, measurements over oceans and at latitudes higher than 50° were not used. Finally, upper and lower thresholds of 1500 and 2000 ppb were set on the SCIAMACHY-retrieved XCH_4.

[34] As a consequence of these filters and of the instrument characteristics, the density and precision of measurements varies between the XCH_4 data sets. The GOSAT-Proxy retrieval contains about 3 times more observations than the Full Physics retrieval (in particular due to the rejection of retrievals over bright surfaces, such as

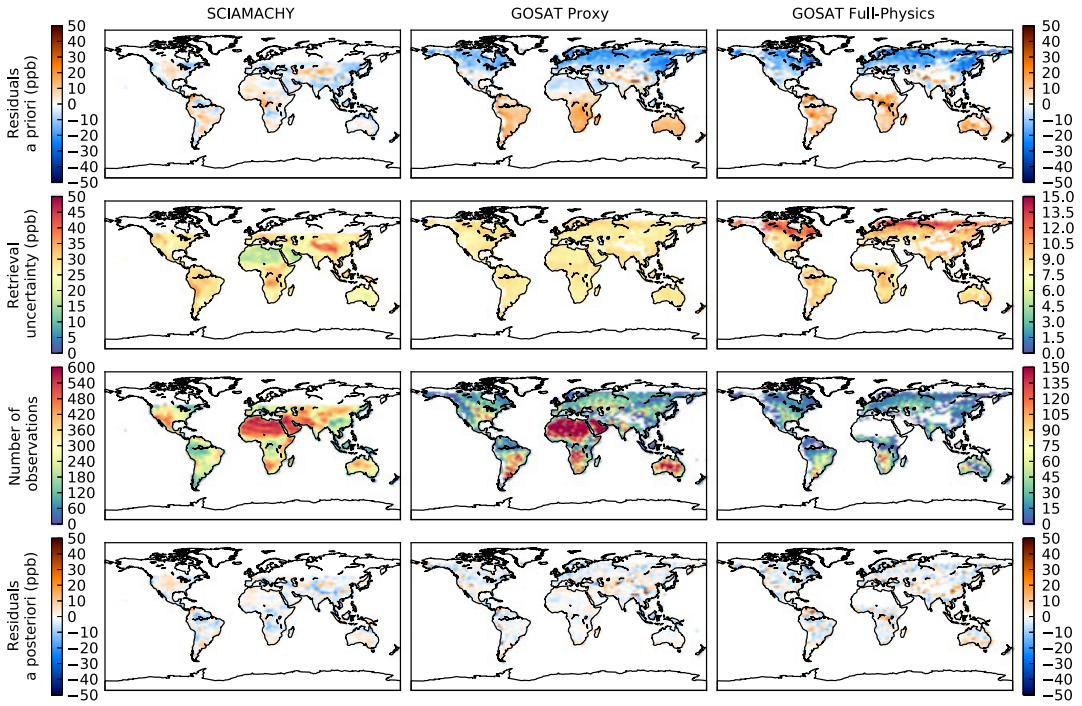

Figure 3. (first row) A priori model-to-observation mismatch, corrected from mean bias. (second row) Retrieval uncertainty. (third row) Number of measurements per 6° × 4° grid box. (last row) A posteriori fit residuals to satellite retrievals. Color bars on the left are for the SCIAMACHY plots (left column), while color bars on the right are for the two GOSAT retrievals (center and right columns).

deserts, in GOSAT-Full Physics). There are also about 4 times more observations in the SCIAMACHY retrieval than in the GOSAT-Proxy. Differences in the number of observations are partly counterbalanced by the differences in retrieval uncertainty. An overview of the amount of data and retrieval uncertainty is summarized in Figure 3 (second and third rows).

[35] Finally, as illustrated in Figure 3 (first row), there are significant differences between the a priori model-to-observation differences: Both GOSAT retrievals show an interhemispheric gradient that is about 25 ppb larger than modeled in TM5. On the contrary, SCIAMACHY retrievals show latitudinal variations that are in better agreement with the model but show larger regional discrepancies, such as significantly higher XCH_4 over the African rain forest and over Central Asia. These differences may point to biases in the retrievals that need to be corrected in a preprocessing stage before the data enter the inversion.

[36] Satellite retrieval biases have been investigated using colocated TCCON measurements, which led to a correction of the GOSAT-Full Physics retrieval by a single coefficient (1.0037, i.e., +6.3 ppb for a 1700 ppb retrieved total column), while no correction needed to be applied to the GOSAT-Proxy retrieval. On the contrary, previous studies [*Bergamaschi et al.*, 2009] and our own experience showed that more complicated bias corrections are required for SCIAMACHY. We apply a bias correction on SCIAMACHY retrievals that consists of a constant and a seasonally varying term with coefficients that optimize the agreement between colocated SCIAMACHY and TCCON measurements for the period 2009–2010. For the seasonal correction we take ECMWF ERA-interim-derived specific humidity averaged over the lowest 3 km of the retrieved column. A more detailed description can be found in Houweling et al. (manuscript in preparation, 2013). In contrast to previous studies [e.g., *Meirink et al.*, 2008b; *Bergamaschi et al.*, 2009], we do not allow the inversion to further optimize this bias correction.

2.3.3. Observation Sampling

[37] Following the cost function $J(\mathbf{x})$ (Equation (1)), the model-to-observation mismatches ($\mathbf{y} - \mathbf{Hx}$) are weighted by the uncertainties stored in matrix $\mathbf{R}$. Individual measurements of the same type (i.e., satellite or in situ) are averaged in 3-hourly time invervals in each model grid box. This is to limit the relative weight of periods with high number of observations in the absence of off-diagonal error correlations in $\mathbf{R}$. The averaged observations are assumed uncorrelated.

[38] In situ observations are compared to modeled CH_4 mixing ratios that are linearly interpolated from the 6° × 4° CH_4 field. Similarly, model-simulated GOSAT and SCIAMACHY retrievals are interpolated to 1° × 1°. These column-mixing ratios are calculated following

$$XCH_4^{\mathrm{mod}} = \frac{1}{p_{\mathrm{surf}}} \sum_{i=0}^{nlev} \delta p_i \left(\mathbf{ak}_i \times CH_{4_i}^{\mathrm{mod}} + (1 - \mathbf{ak}_i) \times CH_{4_i}^{\mathrm{apri}} \right), \quad (3)$$

where $\mathbf{ak}_i$ is the sum of the averaging kernel elements at the layer i. CH_4^{mod} is the model vertical profile, and CH_4^{apri} is the a priori vertical profile of CH_4 used to calculate the retrieval. δp_i represents the pressure thickness of each level, and p_{surf} is the surface pressure. $\mathbf{ak}$ and CH_4^{apri} are provided with the retrieval data sets. The retrieval and the model are not on the same pressure coordinates (the model has 25 vertical layers, while the retrieval has only 6 (GOSAT-Proxy) or 12

Table 2. Inversions Performed and Corresponding Observational Data Sets

Inversion	Observations Used
SURF	NOAA
PRNO	NOAA + GOSAT-Proxy
PR	GOSAT-Proxy
FPNO	NOAA + GOSAT-Full Physics
FP	GOSAT-Full Physics
SCIANO	NOAA + SCIAMACHY
PRc	GOSAT-Proxy (using Proxy and Full Physics filters)

(SCIAMACHY, GOSAT-Full Physics) vertical levels). Hence, it is necessary to interpolate CH_4^{apri}, **ak**, and CH_4^{mod} to the same vertical coordinates. Several interpolation techniques have been tested, without any major impact on XCH_4^{mod} (finally a simple linear interpolation was chosen). It appeared, however, necessary to filter out retrievals whose surface pressure differed significantly from the model surface pressure (i.e., mainly retrievals over isolated mountains).

[39] Like most off-line transport models, the TM5 model tends to underestimate the stratospheric age of air [*Jones et al.*, 2001], resulting in a generally overestimated contribution of upper-stratospheric methane to XCH_4^{mod}. To account for this, we correct model sampled vertical profiles above 50 hPa using a CH_4 climatology based on HALOE/CLAES (Halogen Occultation Experiment/Cryofenic Limb Array Etalon Spectrometer) observations [*Randel et al.*, 1998] when calculating XCH_4^{mod}. This procedure includes a linear correction for the CH_4 increase since the period of observation.

[40] Data uncertainties (ϵ_y) stored in **R** result from a combination of the individual measurement uncertainties, ϵ_{meas}, and of the so-called representation uncertainties, ϵ_{mod} (systematic model-data mismatch caused by the coarseness of the model grid). Representation uncertainties are estimated as using standard deviation of the model local (for in situ observations) or column-averaged (for satellite retrievals) mixing-ratio field in the surrounding grid cells. For surface observations, the sum of measurement and representation uncertainties is used as an estimate for the data uncertainty. For satellite retrievals, the largest of the two uncertainties is used. Measurement uncertainty ϵ_{meas} is set as 3 ppb for all surface observations. For satellite retrievals, the measurement uncertainty is calculated using the retrieval uncertainty (see section 2.3.2).

2.4. Inversions Setup

[41] All inversions were performed for the time period between 1 April 2009 and 31 August 2010. A priori methane concentration fields for April 2009 were taken from an inversion constrained only by surface measurements, covering the period 2007–2010. Fifty iterations of the 4D-VAR algorithm were performed (which ensure a sufficient cost function gradient norm reduction) to ensure a convergence of the optimized emissions and emission uncertainties.

[42] With this common setup, six base inversions were performed for the different measurement data sets, as outlined in Table 2: One inversion constrained only by surface observations (SURF), three inversions constrained by a combination of satellite and surface (NOAA) observations (FPNO, PRNO, and SCIANO), and two inversions constrained only by GOSAT retrievals (FP and PR). SCIAMACHY retrievals contain obvious biases; therefore, it was decided not to perform a SCIAMACHY-only inversion. Finally, an additional inversion (PRc) was also performed, using a GOSAT-Proxy retrievals data set restricted to points where valid GOSAT-Full Physics retrieval are also available,

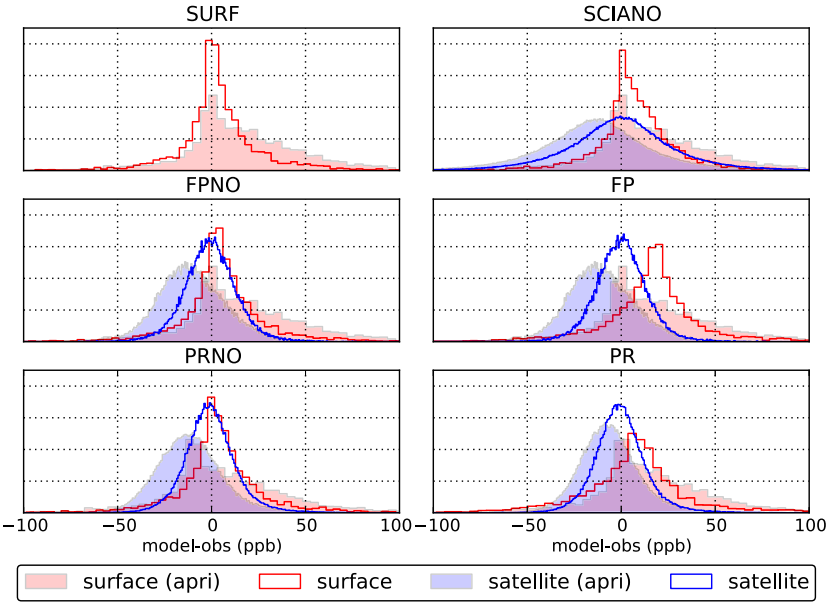

Figure 4. Frequency distribution of fit residuals to NOAA surface observations (red) and to satellite observations (blue) for the a priori model (shaded areas) and for the a posteriori (solid lines). For the FP and PR inversions, NOAA surface concentrations are independent. Histograms are normed by the amount of data they represent.

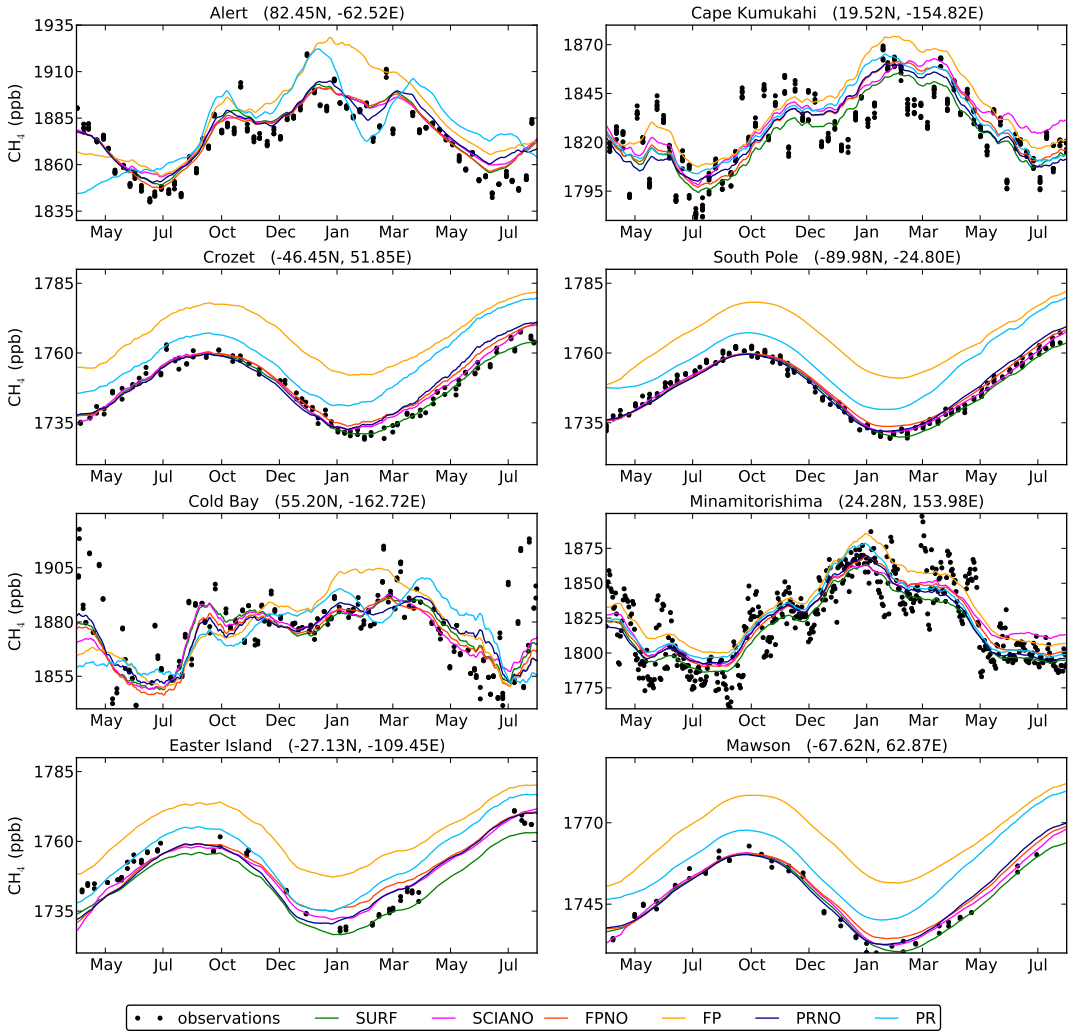

Figure 5. Comparison of model results with measurements at eight background surface sites. Measurements at Alert, Cape Kumukahi, Crozet, and South Pole are assimilated in the SURF, SCIANO, FPNO, and PRNO inversions, while the four other sites are never assimilated.

in order to evaluate the impact of the stricter filtering settings in the Full Physics retrieval.

3. Results

3.1. Statistical Analysis of Fit Residuals

[43] To evaluate the difference in performance between inversions using different measurement data sets, we first analyze the statistics of the fit residuals. Ideally, the posterior fit residuals follow a Gaussian distribution centered around zero, with the width reflecting the posterior concentration uncertainty. In that case the a priori assumptions on flux and observation uncertainty are consistent with the actual level of uncertainty. Shifts in the mean or deviations from Gaussian distributions point to biases or unaccounted error correlations in the observations, in the a priori emissions, or in the transport model.

[44] Frequency distribution plots of fit residuals between modeled concentrations and prescribed surface and satellite measurements are shown in Figure 4 for the six base inversions. The best fit to surface measurements is obtained with the SURF inversion (σ = 26.8 ppb, bias = 4.5 ppb (obs-model)), but the two GOSAT+NOAA inversions (FPNO and PRNO) also reproduce these measurements well (respectively, σ = 26.2 ppb, bias = 5.5 ppb and σ = 28.3 ppb, bias = 4.5 ppb).

[45] The SURF inversion is expected to show the best fit to the NOAA data, because the inversions using satellite data have to satisfy more observational constraints. Differences between fit residuals obtained with and without the use of satellite data point to inconsistencies between these data sets or shortcomings of the transport model.

[46] The SCIANO inversion shows slightly high biased surface mixing ratios (σ = 27.4 ppb, bias = 7.7 ppb), pointing to shortcomings in our ability to correct SCIAMACHY retrieval biases on the basis of a limited number of available TCCON sites. The GOSAT-only inversions, FP and PR, lead to overestimation of surface mixing ratios by 16.9 and 6.9 ppb, respectively, and to increased scatter of the residuals (σ = 33.1 ppb and σ = 39.1 ppb) compared with FPNO and PRNO. It is expected that FP and PR perform less well, since they are not constrained by the surface observations.

However, the presence of a nonnegligible a posteriori bias points to unaccounted systematic errors in these inversions, either in the GOSAT retrievals or in the TM5 model.

[47] The four GOSAT inversions yield similar fits to GOSAT retrievals (σ = 14.7–15.8 ppb, bias = 0–0.6 ppb). The residuals are about a factor of 2 smaller than that for the SCIANO inversion (σ = 32 ppb, bias = 0.3 ppb), which confirms the improved precision of GOSAT compared with SCIAMACHY (see Figure 3). This is true not only for the precision but also the bias, as it should be realized that the SCIANO residuals are obtained after significant bias corrections.

3.2. Reproduction of Observed Methane Variability

[48] Three patterns dominate the variability of the simulated large-scale CH_4 mixing ratio: the seasonal cycle, the latitudinal gradient, and the vertical gradient. While the statistical analysis of fit residuals presented in section 3.1 is useful for quantifying the overall performance of the inversions, it does not provide any insights on how this variability is reproduced in the inversions. Here we take a step further in this direction by analyzing the dominant modes of CH_4 variability using both inversion-optimized and independent data.

3.2.1. Seasonal Cycle

[49] The seasonal cycle of methane is dominated by the seasonal cycle of OH, excepted in regions where emissions show a large seasonal variability (such as natural wetland areas). It is expected that all inversions correctly reproduce the seasonal cycle as observed at background sites. The opposite would imply that either the observations do not provide a sufficient constraint or that the constraint they provide is biased.

[50] Comparisons between surface observations and corresponding inversion estimates are presented in Figure 5. Eight background sites are chosen to cover a wide range of latitudes. Data at four of these sites (Alert, Cape Kumukahi,

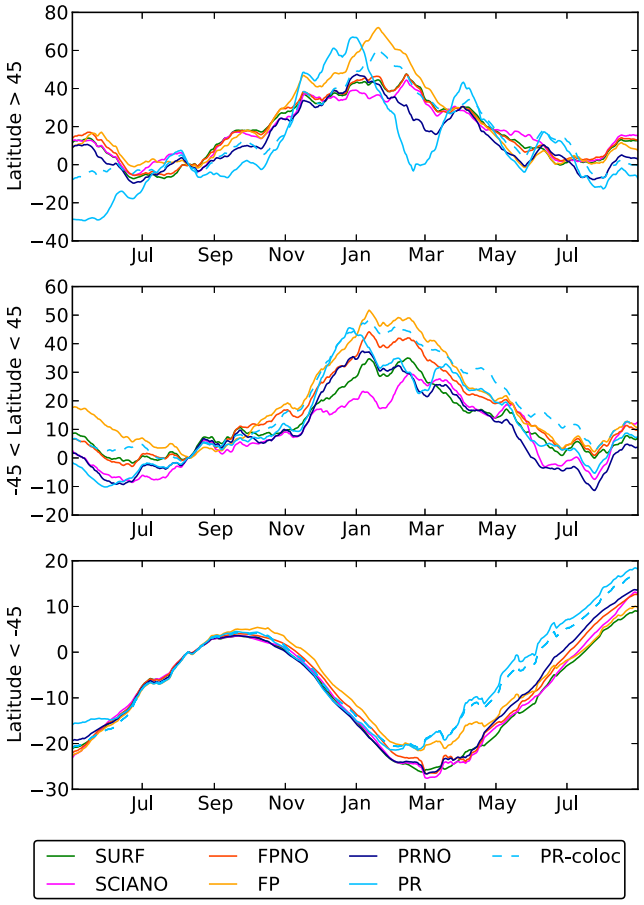

Figure 6. Average seasonal cycle for three latitudinal bands. Model-simulated mixing-ratio fields are evaluated at locations of surface sites used in the SURF inversion. Ten-day moving average is applied to remove the short-term variability.

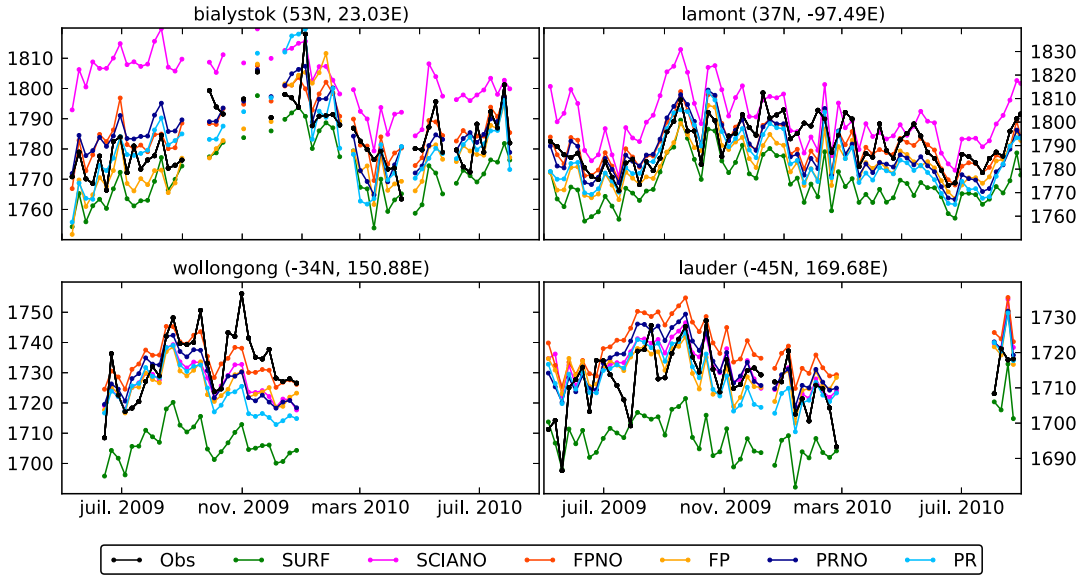

Figure 7. Comparisons between model and measurements at four TCCON sites. Model and measurements are weekly averaged.

Crozet, and South Pole) have been used in the NOAA constrained inversions.

[51] As expected, the four inversions constrained by surface sites reproduce those observations well, which is true also for the independent sites. The two GOSAT-only inversions show overestimated mixing ratios (by 5 to 20 ppb) at all latitudes but more prominently in the Southern Hemisphere. The PR inversion shows a seasonal cycle slightly phase shifted at high latitudes of the Southern Hemisphere (with a winter peak delayed by ~1 month) and strongly deviating from observations at northern high-latitude sites (Alert and Cold Bay).

[52] Figure 6 shows seasonal cycles simulated at all the surface sites used in the inversions, averaged in three zonal bands (corrected by a constant offset corresponding to their mixing ratio on 1 September). Since the SURF inversion reproduces the surface observations very well, it can be used as a reference in the high latitudes (Figure 6, top and bottom). In the low latitudes band (Figure 6, middle) the SURF inversion cannot be used for this purpose because of the limited number of available surface stations in this latitudinal band, which does not allow a proper assessment of its performance.

[53] The seasonal cycles of the SURF, FPNO, and FP inversions are well in phase in all latitude bands. Differences in the amplitude of the seasonal cycle are noted, in particular between FP and SURF at high latitudes. This difference may be due to an insufficient coverage of the GOSAT measurements and therefore does not necessarily imply a bias in the retrieval. Similarly, in the tropics there is only a minor amplitude difference between the seasonal cycles of FP and FPNO, explained by the weak constraints from the surface measurements at those latitudes.

[54] In contrast, the PR inversion shows stronger deviations in the shape of the seasonal cycle compared to the other inversions. In the Northern Hemisphere it leads to an overestimated month-to-month variability that we were able to trace back to unrealistic low retrievals over Siberia, which nonetheless satisfied the default filtering criteria. The more stringent filtering applied to the PRc inversion leads to a much more realistic seasonal cycle in the high-latitude Northern Hemisphere, confirming the influence of data filtering. The contribution of filtering to the phase-shifted seasonal cycle in the high-latitude Southern Hemisphere, however, is much smaller.

[55] The SCIANO inversion does not show significant mismatches in seasonality in the comparisons to surface observations (Figure 5). This might be explained by the seasonal bias correction that is applied to SCIAMACHY retrievals (see section 2.3.2). Despite this correction, somewhat underestimated seasonal cycle amplitudes show up in the tropics as seen most clearly during May–July 2010 in Figure 5 and January 2010 in Figure 6.

3.2.2. Spatial Distribution of Methane

[56] Besides the seasonal cycle, we also verify how well the inversions are able to reproduce the observed methane latitudinal and vertical gradients. Figure 5 shows offsets between the GOSAT-only inversions and the surface observations at high latitudes of the Southern Hemisphere. This could point to biases in the GOSAT retrievals, which would lead to overestimated surface concentrations in the absence of constraints from surface observations. A second possibility is that the TM5 model can be affected by systematic errors, causing it to reproduce correctly either surface or total-column CH_4 but not both at the same time. First we analyze the possibility of a bias in GOSAT by comparing inversion-optimized total-column CH_4 with measurements from the TCCON network of ground-based FTS [*Wunch et al.*, 2010].

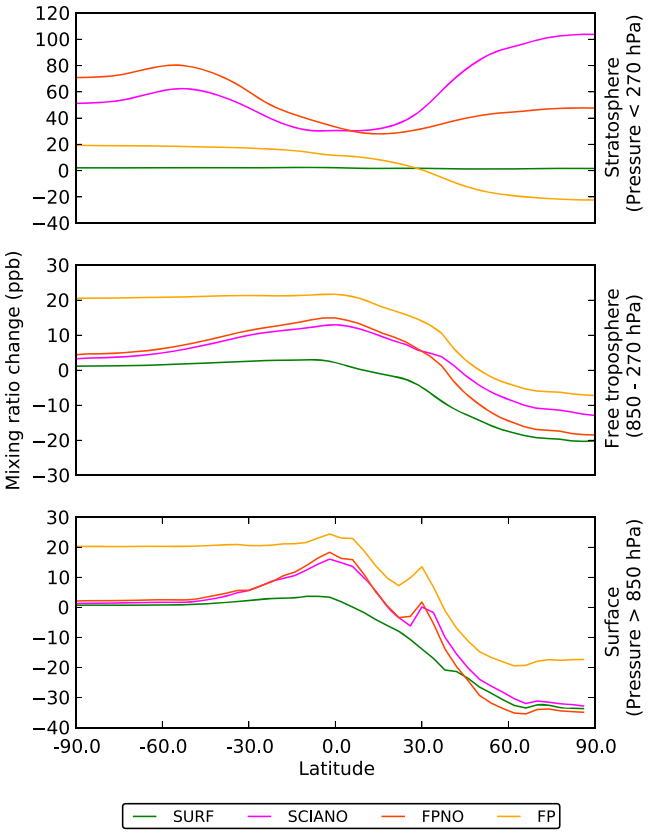

Figure 8. Zonal yearly mixing-ratio adjustment for three pressure ranges: (top) pressures < 270 hPa (stratosphere), (middle) pressures between 850 and 270 hPa (free troposphere), and (bottom) pressures > 850 hPa (planetary boundary layer).

[57] A comparison between model estimates for TCCON retrievals at four TCCON sites is shows in Figure 7. For clarity of the figure, data have been averaged weekly. Overall, GOSAT inversions reproduce TCCON observations very well (with average model-data mismatches between –7 and 10 ppb and standard deviations of these model-data mismatches between 8 and 11 ppb), in line with the good agreement between TCCON and GOSAT XCH_4 reported by *Schepers et al.* [2012]. On the contrary, the SURF inversion shows a systematic underestimation of the total columns by ~20 ppb at the Southern Hemispheric TCCON sites Wollongong and Lauder (and by ~10 ppb in Northern Hemispheric sites). Concerning SCIAMACHY, the SCIANO inversion leads to a pronounced overestimation of TCCON observations in some Northern Hemispheric sites (such as Bialystok, shown in Figure 7) in the first half of the inversion, whereas it shows good agreement with the observations in the second part (after January 2010).

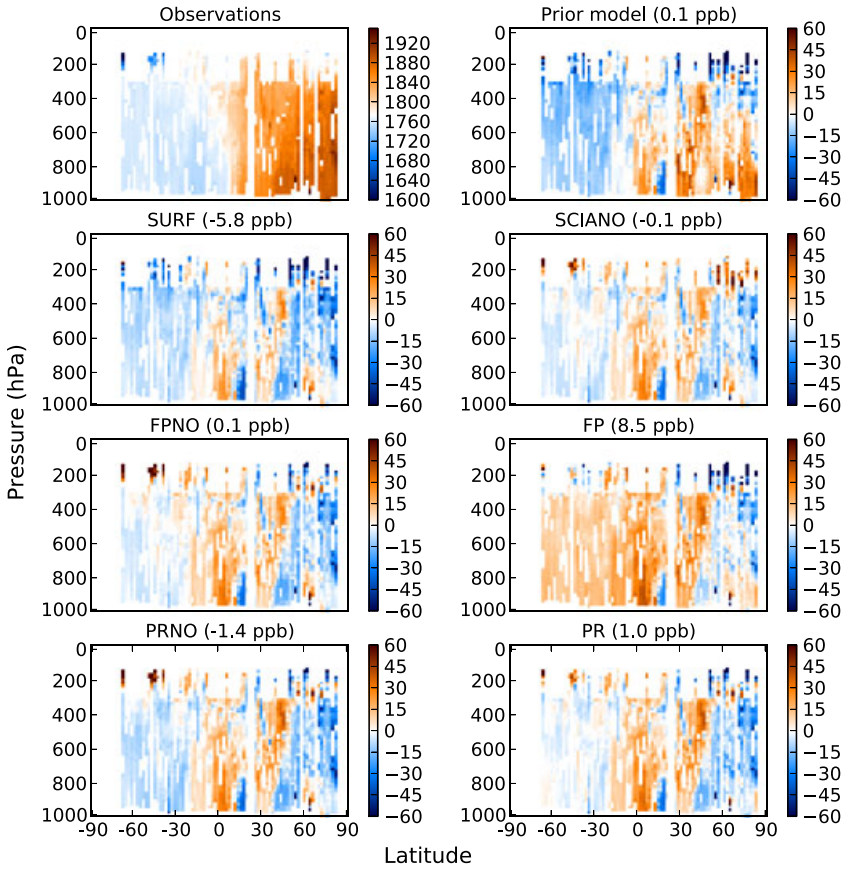

Figure 9. Fit residuals (model-obs) between results from inversions and measurements from the HIPPO campaigns 2 and 3. The value in the title of each plot is the average offset (TM5-obs) for the corresponding simulation.

[58] The sparse global coverage of the TCCON network provides only a limited representation of the Earth's atmosphere; therefore, the good comparison between TCCON and GOSAT is not in itself proof that GOSAT data are totally bias free. It nonetheless permits to exclude the possibility of a global uniform bias of GOSAT retrievals. To further investigate how the inversions deal with the different types of observational constraints, we compare the inversion-optimized vertical gradients in three layers of the atmosphere.

[59] Surface observations are very sensitive to methane variability in the planetary boundary layer and, for background sites, to the variability of the whole troposphere. They are on the contrary not sensitive to methane variability in the stratosphere. In contrast, GOSAT and SCIAMACHY (and TCCON) retrievals are mostly sensitive to the free troposphere and to the lower stratosphere. In Figure 8, we have therefore decomposed the atmosphere in three altitude layers, representing approximately the planetary boundary layer, the free troposphere, and the stratosphere. In each of these layers, and for each simulation, we have calculated the average latitudinal gradient. To limit the number of lines in the figure, we left out the PR and PRNO inversions as they behave similar to, respectively, the FP and FPNO inversions.

[60] The free troposphere (Figure 8, middle) shows adjustments of the latitudinal gradients compared to the prior that are close to what is seen at the surface (Figure 8, bottom). The FP inversion differs from the SURF inversion mostly by an offset of 20 ppb in the Southern Hemisphere and 10 to 15 ppb in the Northern Hemisphere. In the FPNO and SCIANO inversions the additional constraints provided by the surface measurements reduce the difference with the SURF inversions at midlatitudes to high latitudes where the density of surface sites is highest. FPNO and SCIANO are nevertheless able to satisfy the observational constraints on the total column by increasing the methane concentration in the stratosphere. Since our inversion setup does not allow optimization of the atmospheric lifetime of methane, these variations in the vertical profile are obtained by an adjustment of the initial concentration field in the lower stratosphere, which, due to the slow mixing at those altitudes, persists throughout the inversion period.

[61] For a more extensive validation of our results, we also compared our inversion-optimized CH_4 concentrations to measurements from the HIAPER Pole-to-Pole Observations (HIPPO) aircraft campaigns, which provide north-south transects of the troposphere above the Pacific Ocean. We compare our model results to measurements from the HIPPO campaigns 2 and 3 [*Wofsy*, 2011] that coincide with our inversion period (Figure 9). These comparisons show that all simulations, including the prior model, overestimate the methane mixing ratio by 20 to 40 ppb in the lower tropical troposphere. This overestimation extends to the whole tropical troposphere in the SCIAMACHY and GOSAT inversions. The use of surface observations in the FPNO, PRNO, and SCIANO inversions forces the CH_4

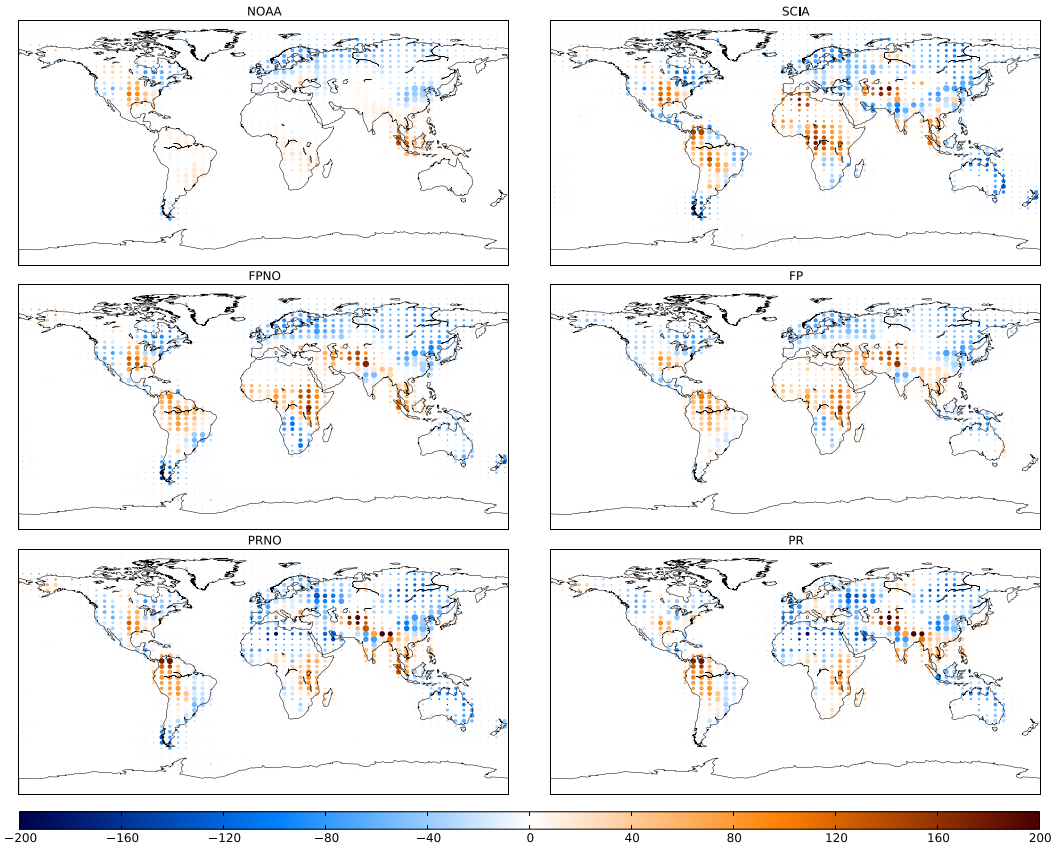

Figure 10. A posteriori emissions compared with emissions a priori for the six inversions. The size of the dots represents the strength of the a priori emissions, while the color describes the percentage emissions change.

mixing ratio to lower values outside the tropics, while in the PR and FP inversions, the CH_4 mixing ratio remains high at Southern Hemisphere high latitudes. This is in general agreement with our interpretation of the surface observations and TCCON comparisons.

3.3. Inversion-Optimized Fluxes

[62] In this section we investigate how the differences in spatial and temporal gradients of CH_4 as analyzed in the previous sections translate into differences in inversion-derived surface fluxes.

[63] Optimized methane emissions are shown in Figure 10, in a layout that emphasizes inversion-derived modifications of the a priori fluxes that are significant in both absolute and relative sense. Emissions on the model grid are commonly not well resolved by the measurements and can therefore be difficult to interpret. More robust flux adjustments, integrated over larger regions, are shown in Figure 11.

[64] The estimated global yearly total emissions are highly consistent across the inversions, ranging from –2.4% to +2.7% of the a priori emissions. This is expected for the inversions constrained by surface observations, since those observations provide an accurate constraint on the annual methane growth rate. The total emissions inferred from the GOSAT-only inversions are also very similar (at least when the strict filtering settings are used for the GOSAT-Proxy inversion, PRc), which confirms that there is no significant global bias in the GOSAT retrievals. The inconsistencies between low and high altitude adjustments that were discussed in the previous section do not strongly influence the estimated global fluxes.

[65] Integrated over large scales, all inversions yield an increase of tropical emissions (from +31 Tg CH_4/yr for SURF up to 63 Tg CH_4/yr for FPNO), compensated by an equivalent reduction of CH_4 emissions in Northern Hemisphere temperate and high latitudes (–27 Tg CH_4/yr for FP and PRc, down to –49 Tg CH_4/yr for the SCIANO inversion). The use of satellite observations allows a better resolution of tropical emissions, as illustrated in Figure 10. While the SURF inversion shows a homogeneous adjustment of the emissions across the tropical continents (except for Indonesia), the satellite inversions show more variations, with the tropical emission increase attributed mainly to four regions: the Amazon basin, Central Africa (particularly the Victoria Lake region), Indonesia, and Central Asia (Iran, Afghanistan, etc.).

[66] In line with the latitudinal concentration gradients shown in section 3.2.2, the joined inversions of satellite and surface observations increase the ratio between the tropical and extratropical emissions. This also causes minor regional inconsistencies, such as negative emissions over Patagonia. This is one of the degrees of freedom by which the inversion can satisfy the incompatible constraints of high satellite-retrieved XCH_4 in the tropics and comparably low surface measurements at temperate to high latitudes. Without the

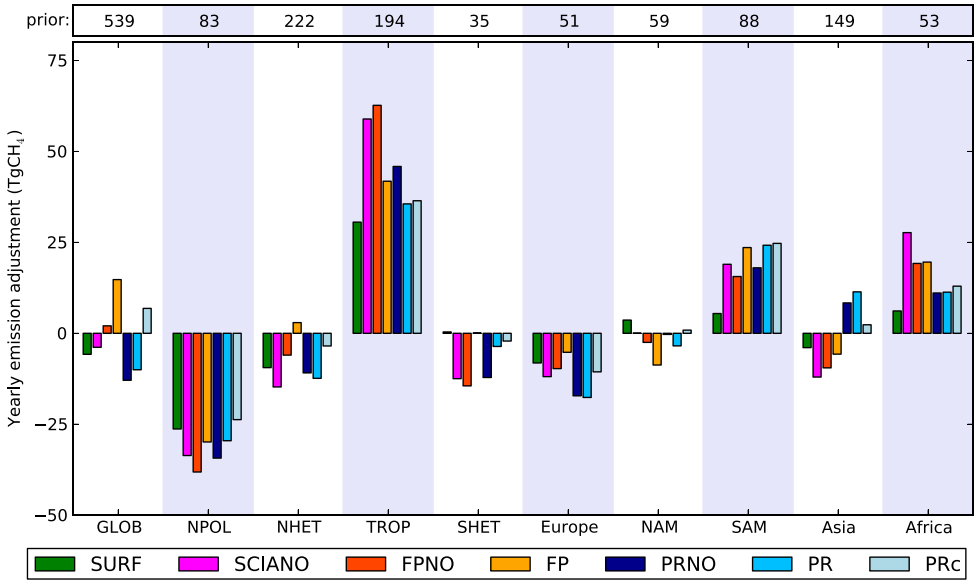

Figure 11. (top) A priori methane emissions and (bottom) emission adjustments for regions defined in Figure 2.

strong observational constraints at high latitudes, FP and PR (and PRc) lead to more homogeneous emission adjustments.

[67] Figure 10 shows negative emissions (contours below –100% adjustment of the a priori flux) for the proxy inversions over North Africa (including the Arabic Peninsula) and Western Russia. This flux adjustment coincides with the anomalous seasonal variability found in the Northern Hemisphere in the PR and PRNO inversions (see section 3.2.2) and disappears using the stricter filtering settings of the PRc inversion, as explained earlier (see also Figure 11).

[68] The GOSAT-Proxy inversions show larger emissions over Asia than the Full Physics. This may be explained by regional larger values of XCH_4 in the GOSAT-Proxy retrieval than in the GOSAT-Full Physics, which cannot be fully explained by differences in data selection since PRc shows intermediate Asian emissions. These differences between the two retrievals have been reported by *Schepers et al.* [2012], who explain it by shortcomings in the model-derived CO_2 fields that are used to translate the GOSAT-retrieved proxy ratios into XCH_4. Although this should also affect the SCIAMACHY retrievals, the SCIANO inversion does not show similar flux adjustments over India. This may be explained by either the larger retrieval uncertainty of SCIAMACHY or a regional bias correction of SCIAMACHY retrievals coincidentally compensating errors in $CO_{2_{\text{model}}}$. It confirms the added value of the Full Physics retrieval, which does not require such corrections and allows a quasi-independent verification of the proxy retrievals.

4. Discussion

[69] We have investigated the application of GOSAT XCH_4 retrievals to atmospheric inverse modeling of the global sources and sinks of CH_4 and compared the performance of inversions using GOSAT to the use of SCIAMACHY and surface measurements. For all the observational data sets included in the analysis, we find that our a priori emissions are too low in the tropics (by 35 to 64 Tg CH_4/yr) and too high in the Northern Hemisphere midlatitudes to high latitudes (by 39 to 49 Tg CH_4/yr). This shift is consistent with previous inverse modeling analyses of the global CH_4 cycle using the TM5 model (and its previous versions TM2, TM3, and TM4) in applications to both satellite and surface measurements [*Houweling et al.*, 1999; *Hein et al.*, 1997; *Bergamaschi et al.*, 2009].

[70] This overestimated north-south gradient of methane in the a priori simulations was hypothesized to be caused in part by a too slow interhemispheric exchange in the TM family of transport models, which was recently confirmed by simulations of SF_6 conducted as part of the TRANSCOM-CH4 model intercomparison experiment [*Patra et al.*, 2011]. In this study, we have accounted for this model shortcoming by introducing a parameterization of horizontal diffusion, which was used to calibrate the interhemispheric exchange of TM5 based on the observed SF_6 gradient. This calibration shifted the inverse modeling-derived CH_4 emissions by about 40 Tg/yr from the Southern to the Northern Hemisphere. Despite this adjustment, which shows up largely as a shift across tropical latitudes, an additional correction from the extratropics to the tropics is needed, strengthening the evidence that the overestimated latitudinal gradient has also a contribution from a priori underestimated tropical emissions.

[71] Compared to an inversion using only surface observations, inversions constrained by satellite retrievals lead to an increased resolution of tropical and Southern Hemispheric emissions. Integrated over the tropics, the GOSAT measurements confirm conclusions drawn in the past using SCIAMACHY about underestimated tropical emissions. However, on the subcontinental to regional scales, differences between the inversion-estimated fluxes are still rather large and also larger than the single inversion-derived regional flux uncertainties. In the remainder of this section, we discuss the possible causes of these differences and summarize the most robust outcomes of our inversion intercomparison.

[72] As described in section 3.3, in the tropics, the combined use of surface and satellite measurements leads to systematically higher tropical emissions compared with the use of only surface measurements or only satellite retrievals. The opposite is found at higher latitudes where the combined use of surface and satellite measurements leads to stronger emission reductions compensating for the tropical increase. Since the options for emission reductions in the Southern Hemisphere are limited, this causes unrealistic negative emissions over Patagonia. Meanwhile, inversions combining surface and satellite observations lead to larger adjustments of the methane vertical distribution, which may not improve the representation of the stratosphere (section 3.2.2). These adjustments of the vertical profile and of the tropical/extratropical emission balance are two symptoms of the fact that our transport model is unable to reconcile observational constraints on surface and total-column CH_4.

[73] One cause of this difficulty could be the existence of remaining regional biases in the CH_4 retrievals. Given the overall good consistency between SCIAMACHY and GOSAT, it seems unlikely that instrumental problems play an important role. In fact, our results provide important confirmation of the findings of SCIAMACHY that have been reported in the past. On the retrieval side, however, there is the possibility of common biases, for example, due to spectroscopic uncertainties. Common errors in the treatment of aerosols are not very likely, because the proxy and full physics retrievals are very different approaches to correct perturbations of the optical path due to aerosol scattering. In addition, the good performance of the two GOSAT retrievals is confirmed by a good agreement to TCCON retrievals [*Butz et al.*, 2011; *Schepers et al.*, 2012]. Nevertheless, important uncertainties remain due to the limited coverage of the TCCON network in particular at southern latitudes and in the tropics. The SCIAMACHY bias correction, although reasonably effective at this stage, strongly relies on the global representativity of the TCCON network.

[74] A second possible cause is errors in the transport model itself that would make it difficult to reproduce well in the same time two different types of observations. The joint constraints of surface observations and satellite retrievals would be accommodated easier with less efficient intrahemispheric mixing that would reduce the exchange of methane between the tropics and Southern Hemispheric extratropics. This exchange has been increased by introducing horizontal diffusion (section 2.1) to speed up the interhemispheric mixing. It is difficult to evaluate the impact of the added diffusion on the performance of the transport model at smaller scales. Sensitivity tests did not show significant changes except for minor modifications of the seasonal cycle near the surface in the tropics. Regionally, the tropical seasonal cycle of methane shows a significant influence from the seasonal dynamics of the ITCZ, which explains the influence of horizontal diffusion since it is coupled to convective mass fluxes. More tropical measurements would be needed, however, to quantify if this results in an overall gain or loss in performance. Besides horizontal mixing there is also the possibility that vertical mixing or stratosphere-troposphere exchange plays a role.

[75] Finally, a third and interesting candidate to explain this systematic mismatch between surface and column-mixing ratios is atmospheric chemistry. Our inversion setup has been simplified by prescribing the photochemical sinks as hard constraints, motivated by the limited available information in satellite and surface measurements to independently constrain surface sources and atmospheric sinks. Besides tropospheric OH, the combined impact of uncertainties in stratospheric chemistry and stratosphere-troposphere exchange also has the potential to significantly modify the simulation of XCH_4. On the other hand, the adjustments of the lower stratosphere as shown in Figure 8 do not seem to make the model more realistic, suggesting that the required modifications may be outside the uncertainty range.

[76] Comparisons with HIPPO observations (Figure 9) show that a relative overestimation of tropical CH_4 may be present in all simulations, including the prior model and the SURF inversion. This could support the hypothesis of transport model errors in the tropics but would need to be confirmed by measurements at other longitudes and other seasons. An in-depth analysis of the possible contribution of chemistry, transport, and retrieval uncertainties discussed here is outside the scope of this study. However, it is realized that such an analysis could provide valuable insights and is therefore planned as part of a follow-up publication.

[77] Despite the significance of discussion above for the methane budget in the midlatitude to high-latitude Southern Hemisphere, it is important to realize that the total uncertainty introduced by this potential bias is low. For example, emissions integrated over the tropical band show only 8% difference between FP and FPNO and 5% difference between PR and PRNO. Our ratio of tropical to nontropical emissions is also in the range of what was published in earlier studies. In *Bousquet et al.* [2010] the emissions between 30°N and 30°S account for 54% of the global annual emissions based on surface measurements, compared to 59% to 63% in our inversions. *Bergamaschi et al.* [2009] report that low-latitude emissions represent 62% of the total methane emissions, using the TM5-4DVAR applied to SCIAMACHY retrievals for the year 2004. Depending on the satellite data set used, we estimate the emission from tropical South America at 66 to 74 Tg CH_4/yr, which is similar to estimates reported by *Mikaloff Fletcher et al.* [2004] and *Frankenberg et al.* [2008]. Our emission estimates are also in good agreement with those of *Fraser et al.* [2012], on the basis of a different GOSAT-Proxy retrieval [*Parker et al.*, 2011]: We find total CH_4 emissions in South America ranging from 94 (SURF) to 113 (PRc) Tg CH_4/yr, which is in line with their estimates (99–105 Tg CH_4/yr). Our emissions in Africa (60 Tg CH_4/yr (SURF), 81 Tg CH_4/yr (SCIANO), and 65–73 Tg CH_4/yr (GOSAT inversions)) are slightly lower than what they report (83.5–92.5 Tg CH_4/yr), but the region definitions are not totally similar and can easily explain these differences.

[78] The use of two different retrieval data sets derived from the same satellite instrument provides a good opportunity to compare the added value of each retrieval method for CH_4 inverse modeling. The Proxy retrieval approach allows for a more extensive coverage and therefore should provide stronger constraints on CH_4 emissions. However, the use of GOSAT-Full Physics retrievals leads to a more realistic temporal variation of the surface mixing ratio in the Northern Hemisphere and more plausible emission estimates over Europe and the Sahara. The reduced accuracy of the proxy

method can to some extent be compensated by stricter data selection but at the cost of losing the extended coverage. In the high-latitude Southern Hemisphere the GOSAT-Proxy retrieval shows a phase-shifted seasonal cycle, which is not sensitive to filtering settings (Figure 5). This currently limits the added value of the GOSAT-Proxy inversions compared with the Full Physics approach. However, ongoing development of the retrieval codes may change this situation in the future. From the perspective of inverse modeling, the availability of data sets from alternative retrieval techniques is highly valuable for assessing the robustness of inversion-derived emission estimates, as demonstrated in this study.

5. Conclusion

[79] We have performed an intercomparison of CH_4 inversions constrained by three different data products of satellite-retrieved XCH_4: the SCIAMACHY IMAPv5.5 retrieval [*Frankenberg et al.*, 2011] and the GOSAT RemoteC Proxy and Full Physics retrievals [*Butz et al.*, 2010, 2011; *Schepers et al.*, 2012]. The GOSAT inversions have been carried out with and without a set of surface observations from the NOAA ESRL network [*Dlugokencky et al.*, 2013]. Inversion-derived emissions were compared and evaluated using different sets of independent observations. The main goals were to evaluate the performances of GOSAT methane inversions in comparison to earlier published SCIAMACHY inversions and to further investigate the role of measurement uncertainty in relation to other uncertainties, such as those of the a priori CH_4 sources and sinks and the transport model that was used. Specific attention is paid to the comparison of inversions using the Proxy or Full Physics retrieval of GOSAT.

[80] Despite important differences between the GOSAT and SCIAMACHY instruments and between the Proxy and the Full Physics retrieval methods, it is found that all satellite inversions lead to very comparable large-scale adjustments of the a priori emissions. These results confirm earlier findings using SCIAMACHY [*Bergamaschi et al.*, 2009; *Frankenberg et al.*, 2011], pointing, for example, to increased emissions from the tropics. An important difference between the satellite instruments is the improved accuracy of GOSAT, which allows an inversion setup without the co-optimization of bias coefficients, as commonly used for SCIAMACHY to improve the internal consistency. The absence of such bias corrections in the GOSAT inversions strengthens the conclusions based on the new retrievals.

[81] As expected, the largest added value of satellites is found over tropical continents where satellites allow an important extension of measurement coverage. Compared to a reference inversion constrained only by surface observations, inversions using satellite retrievals point to higher emissions in South America (Amazon basin) and Central Western Africa (Victoria Lake region) than accounted for in our prior estimate. Although our inversion setup provides limited process-specific information, the underestimated emissions are likely related to tropical wetlands, which are the most uncertain. The satellite inversions also show an area of strong methane emissions over Central Asia, which could be related to the use of fossil fuel or geologic emissions. Other important emission changes common to all inversions include reductions of emissions in Eastern China and the Northern Hemisphere high latitudes.

[82] The comparisons to independent measurements, such as TCCON ground-based FTS and the HIPPO aircraft campaigns, show the best agreement using the GOSAT-Full Physics retrievals. Comparable fits to observations are also obtained using SCIAMACHY but rely on significant bias corrections. The reduced coverage of the GOSAT-Full Physics retrieval compared to SCIAMACHY is compensated by the improved quality of the retrievals. For the GOSAT-Proxy retrieval, some unrealistic variations in XCH_4 were found over Asia, which led to significantly perturbed seasonal variations in the inversion-optimized fluxes. A stricter filtering of the GOSAT-Proxy retrieval avoids these artifacts. However, it also significantly reduces the measurement coverage, which is considered an important strength of the Proxy method compared with the Full Physics method.

[83] Comparisons of inversions using only surface or satellite data point to remaining inconsistencies between the constraints imposed by surface and total-column measurements. Comparisons of the satellite data to TCCON ground-based FTS measurements indicate that the problem is unlikely to be caused by the satellite retrievals. Alternative possible explanations are shortcomings in the atmospheric transport model or in the representation of the atmospheric oxidation of methane, which is not optimized in the current inversion setup. This highlights the need for further developments not only of satellite retrievals but also of the chemistry and transport models that are used for their interpretation. Developments on the modeling side rely critically on the availability of in situ measurements. To resolve the current inconsistency between surface and total-column measurements would greatly benefit from extended in situ monitoring of surface and total-column CH_4 over tropical continents.

[84] Further research will focus on the use of satellites for studying interannual variations and trends of methane. The overall good agreement between inversion results obtained using SCIAMACHY and GOSAT are an encouraging step in this direction.

[85] **Acknowledgments.** This project was funded by the Dutch NWO under grant 865.07.007. Funding from ESA's Climate Change Initiative on GHGs (Sandrine Guerlet) and the European Commission's 7th framework program under grant agreement 218793 (Sandrine Guerlet and Remco Scheepmaker) is acknowledged. Dinand Schepers is supported by the gebruikersondersteuning ruimteonderzoek program of NWO through project ALW-GO-AO/21. André Butz has been supported by Deutsche Forschungsgemeinschaft (DFG) through the Emmy-Noether Programme (grant BU2599/1-1, RemoteC). We thank SURFsara (www.surfsara.nl) for the support in using the Dutch national super computer Huygens. We thank the data providers: Access to the GOSAT data was granted through the 2nd GOSAT research announcement jointly issued by JAVA, NIES, and MOE; surface observations from the NOAA/CMDL network were obtained from the website http://www.esrl.noaa.gov/gmd/dv/iadv; TCCON data were obtained from the TTCON DATA Archive, operated by the California Institute of Technology (http://tccon.ipac.caltech.edu); we thank Steven Wofsy (Harvard University) for providing the HIPPO data used in the paper and for his useful suggestions.

References

Bange, H. W., T. G. Bell, M. Cornejo, A. Freing, G. Uher, R. C. Upstill-Goddard, and G. Zhang (2009), MEMENTO: A proposal to develop a database of marine nitrous oxide and methane measurements, *Environ. Chem.*, *6*, 195–197.

Basu, S., et al. (2013), Global CO_2 fluxes estimated from GOSAT retrievals of total column CO_2, *Atmos. Chem. Phys. Disc.*, *13*, 4535–4600.

Bergamaschi, P., et al. (2009), Inverse modeling of global and regional CH4 emissions using SCIAMACHY satellite retrievals, *J. Geophys. Res.*, *114*, D22301, doi:10.1029/2009JD012287.

Bousquet, P., et al. (2006), Contribution of anthropogenic and natural sources to atmospheric methane variability, *Nature*, *443*, 439–443.

Bousquet, P., et al. (2010), Source attribution of the changes in atmospheric methane for 2006–2008, *Atmos. Chem. Phys. Discuss.*, *10*, 27,603–27,630.

Buchwitz, M., et al. (2005), Atmospheric methane and carbon dioxide from SCIAMACHY satellite data: Initial comparison with chemistry and transport models, *Atmos. Chem. Phys.*, *5*, 941–962.

Butz, A., O. P. Hasekamp, C. Frankenberg, J. Vidot, and I. Aben (2010), CH_4 retrievals from space-based solar backscatter measurements: Performance evaluation against simulated aerosol and cirrus loaded scenes, *J. Geophys. Res.*, *115*, D24302, doi:10.1029/2010JD014514.

Butz, A., et al. (2011), Toward accurate CO_2 and CH_4 observations from GOSAT, *Geophys. Res. Lett.*, *38*, L14812, doi:10.1029/2011GL047888.

Crevoisier, C., D. Nobileau, A. M. Fiore, R. Armante, A. Chédin, and N. A. Scott (2009), Tropospheric methane in the tropics—First year from IASI hyperspectral infrared observations, *Atmos. Chem. Phys.*, *9*, 6337–6350.

Crutzen, P. J., R. Hein, and M. Heimann (1997), An inverse modeling approach to investigate the global atmospheric methane cycle, *Global Biogeochem. Cycles*, *11*, 43–76.

Dee, D. P., et al. (2011), The ERA-Interim reanalysis: Configuration and performance of the data assimilation system, *Q. J. R. Meteorol. Soc.*, *137*, 553–597, doi:10.1002/qj.828.

Denman, K. L., et al. (2007), Couplings between changes in the climate system and biogeochemistry, in *Climate Change 2007: The Physical Science Basis. Contribution of the Working Group I to the Fourth Assessment Report of the Intergovernmental Panel on Climate Change*, edited by S. Solomon et al., 996 pp., Cambridge University Press, Cambridge, United Kingdom and New York, NY, USA.

Dentener, F., M. van Weele, M. Krol, S. Houweling, and P. van Velthoven (2003), Trends and inter-annual variability of methane emissions derived from 1979–1993 global CTM simulations, *Atmos. Chem. Phys.*, *3*, 73–88.

Dlugokencky, E. J., P. M. Lang, A. M. Crotwell, K. A. Masarie, and M. J. Crotwell (2013), Atmospheric Methane Dry Air Mole Fractions from the NOAA ESRL Carbon Cycle Cooperative Global Air Sampling Network, 1983-2012, Version: 2013-08-28. Path: ftp://aftp.cmdl.noaa.gov/data/trace_gases/ch4/flask/surface/.

Dlugokencky, E. J., S. Houweling, L. Bruhwiler, K. A. Masarie, P. M. Lang, J. B. Miller, and P. P. Tans (2003), Atmospheric methane levels off: Temporary pause or a new steady-state?, *Geophys. Res. Lett.*, *30*, 1992, doi:10.1029/2003GL018126.

Dueck, T. A., et al. (2007), No evidence for substantial aerobic methane emission by terrestrial plants: A ^{13}C-labelling approach, *The New Phytologist*, *175*, 29–35.

Errico, R. M. (1997), What is an adjoint model?, *Bull. Amer. Meteorol. Soc.*, *78*, 2577–2591.

Etiope, G., and R. W. Klusman (2002), Geologic emissions of methane to the atmosphere, *Chemosphere*, *49*, 777–789.

Etiope, G., and A. V. Milkov (2004), A new estimate of global methane flux from onshore and shallow submarine mud volcanoes to the atmosphere, *Environ. Geol.*, *46*, 997–1002.

Etiope, G., K. R. Lassey, R. W. Klusman, and E. Boschi (2008), Reappraisal of the fossil methane budget and related emission from geologic sources, *Geophys. Res. Lett.*, *35*, L09307, doi:10.1029/2008GL033623.

Fisher, M., and D. J. Lary (1995), Lagrangian four-dimensional variational data assimilation of chemical species, *Q. J. R. Meteorol. Soc.*, *121*, 1681–1704.

Forster, F., et al. (2007), Changes in atmospheric constituents and in radiative forcing, in *Climate Change 2007: The Physical Science Basis. Contribution of the Working Group I to the Fourth Assessment Report of the Intergovernmental Panel on Climate Change*, edited by S. Solomon et al., p. 212, Cambridge University Press, Cambridge, United Kingdom and New York, NY, USA.

Francey, R. J., L. P. Steele, R. L. Langenfelds, and B. C. Pak (1999), High precision long-term monitoring of radiatively active and related trace gases at surface sites and from Aircraft in the Southern Hemisphere Atmosphere, *J. Atmos. Sci.*, *56*, 279–285.

Frankenberg, C., J. F. Meirink, M. van Weele, U. Platt, and T. Wagner (2005a), Assessing methane emissions from global space-borne observations, *Science*, *308*, 1010–1014.

Frankenberg, C., U. Platt, and T. Wagner (2005b), Iterative maximum a posteriori (IMAP)-DOAS for retrieval of strongly absorbing trace gases: Model studies for CH_4 and CO_2 retrieval from near infrared spectra of SCIAMACHY onboard ENVISAT, *Atmos. Chem. Phys.*, *5*, 9–22.

Frankenberg, C., I. Aben, P. Bergamaschi, E. J. Dlugokencky, R. van Hees, S. Houweling, P. van der Meer, R. Snel, and P. Tol (2011), Global column-averaged methane mixing ratios from 2003 to 2009 as derived from SCIAMACHY: Trends and variability, *J. Geophys. Res.*, *116*, D04302, doi:10.1029/2010JD014849.

Frankenberg, C., P. Bergamaschi, A. Butz, S. Houweling, J. F. Meirink, J. Notholt, A. K. Petersen, H. Schrijver, T. Warneke, and I. Aben (2008), Tropical methane emissions: A revised view from SCIAMACHY onboard ENVISAT, *Geophys. Res. Lett.*, *35*, L15811, doi:10.1029/2008GL034300.

Fraser, A., et al. (2012), Estimating regional methane surface fluxes: The relative importance of surface and GOSAT mole fraction measurements, *Atmos. Chem. Phys. Disc.*, *12*, 30,989–31,030.

Hansen, J., M. Sato, R. Ruedy, A. Lacis, and V. Oinas (2000), Global warming in the twenty-first century: An alternative scenario, *P. Natl. Acad. Sci. USA*, *97*, 9875–9880.

Hein, R., P. J. Crutzen, and M. Heimann (1997), An inverse modeling approach to investigate the global atmospheric methane cycle, *Global Biogeochem. Cycles*, *11*, 43–76.

Höglund-Isaksson, L. (2012), Global anthropogenic methane emissions 2005–2030: Technical mitigation potentials and costs, *Atmos. Chem. Phys. Disc.*, *12*, 11,275–11,315.

Hooghiemstra, P. B., M. C. Krol, J. F. Meirink, P. Bergamaschi, G. R. van der Werf, P. C. Novelli, I. Aben, and T. Röckmann (2011), Optimizing global CO emission estimates using a four-dimensional variational data assimilation system and surface network observations, *Atmos. Chem. Phys.*, *11*, 4705–4723.

Hooghiemstra, P. B., M. C. Krol, P. Bergamaschi, A. T. J. de Laat, G. R. van der Werf, P. C. Novelli, M. N. Deeter, I. Aben, and T. Röckmann (2012), Comparing optimized CO emission estimates using MOPITT or NOAA surface network observations, *J. Geophys. Res.*, *117*, D06309, doi:10.1029/2011JD017043.

Houweling, S., T. Kaminski, F. Dentener, J. Lelieveld, and M. Heimann (1999), Inverse modeling of methane sources and sinks using the adjoint of a global transport model, *J. Geophys. Res.*, *104*, 26,137–26,160.

Jones, D. B. A., A. E. Andrews, H. R. Schneider, and M. B. McElroy (2001), Constraints on meridional transport in the stratosphere imposed by the mean age of air in the lower stratosphere, *J. Geophys. Res.*, *106*, 10,243–10,256.

Keppler, F., J. T. G. Hamilton, M. Brass, and T. Röckmann (2006), Methane emissions from terrestrial plants under aerobic conditions, *Nature*, *439*, 187–191.

Keppler, F., M. Boros, C. Frankenberg, J. Lelieveld, A. McLeod, A. M. Pirttilä, T. Röckmann, and J.-P. Schnitzler (2009), Methane formation in aerobic environments, *Environ. Chem.*, *6*, 459–465.

Kvenvolden, K. A., and B. W. Rogers (2005), Gaia's breath—Global methane exhalations, *Mar. Petrol. Geol.*, *22*, 579–590.

Lanczos, C. (1950), An iteration method for the solution of the eigenvalue problem of linear differential and integral operators, *J. Res. Nat. Bur. Stand.*, *45*, 255–282.

Law, K. S., and J. A. Pyle (1993), Modeling trace gas budgets in the troposphere: 2. CH_4 and CO, *J. Geophys. Res.*, *98*, 18,401–18,412.

Matthews, E., and I. Fung (1987), Methane emissions from natural wetlands: Global distribution, area and environmental characteristics of sources, *Global Biogeochem. Cycles*, *1*, 61–86.

Meirink, J. F., H. J. Eskes, and A. P. H. Goede (2006), Sensitivity analysis of methane emissions derived from SCIAMACHY observations through inverse modelling, *Atmos. Chem. Phys.*, *6*, 1275–1292.

Meirink, J. F., P. Bergamaschi, and M. C. Krol (2008a), Four-dimensional variational data assimilation for inverse modelling of atmospheric methane emissions: Method and comparison with synthesis inversion, *Atmos. Chem. Phys.*, *8*, 6341–6353.

Meirink, J. F., et al. (2008b), Four-dimensional variational data assimilation for inverse modeling of atmospheric methane emissions: Analysis of SCIAMACHY observations, *J. Geophys. Res.*, *113*, D17301, doi:10.1029/2007JD009740.

Mikaloff Fletcher, S. E., P. P. Tans, L. M. Bruhwiler, J. B. Miller, and M. Heimann (2004), CH_4 sources estimated from atmospheric observations of CH4 and its $^{13}C/^{12}C$ isotopic ratios: 2. Inverse modeling of CH_4 fluxes from geographical regions, *Global Biogeochem. Cycles*, *18*, GB4005, doi:10.1029/2004GB002224.

Montzka, S. A., M. Krol, E. Dlugokencky, B. Hall, P. Jöckel, and J. Lelieveld (2011), Small interannual variability of global atmospheric hydroxyl, *Science*, *331*, 67–69.

Nisbet, R. E. R., et al. (2009), Emission of methane from plants, *P. Roy. Soc. B-Biol. Sci.*, *276*, 1347–1354.

Parker, R., et al. (2011), Methane observations from the Greenhouse Gases Observing SATellite: Comparison to ground-based TCCON data and model calculations, *Geophys. Res. Lett.*, *38*, L15807, doi:10.1029/2011GL047871.

Parrish, D. D., and J. C. Derber (1992), The National Meteorological Center's spectral statistical-interpolation analysis system, *Mon. Weather Rev.*, *120*, 1747–1763.

Patra, P. K., et al. (2011), TransCom model simulations of CH_4 and related species: Linking transport, surface flux and chemical loss with CH_4 variability in the troposphere and lower stratosphere, *Atmos. Chem. Phys.*, *11*, 12,813–12,837.

Peters, W., et al. (2007), An atmospheric perspective on North American carbon dioxide exchange: CarbonTracker, *P. Natl. Acad. Sci. USA*, *104*, 18,925–18,930.

Peters, W., et al. (2010), Seven years of recent European net terrestrial carbon dioxide exchange constrained by atmospheric observations, *Global Change Biology*, *16*, 1317–1337, doi:10.1111/j.1365-2486.2009.02078.x.

Prather, M., M. McElroy, S. Wofsy, G. Russel, and D. Rind (1987), Chemistry of the global troposphere: Fluorocarbons as tracers of air motion, *J. Geophys. Res.*, *92*, 6579–6613.

Querino, C. A. S., C. J. P. P. Smeets, I. Vigano, R. Holzinger, V. Moura, L. V. Gatti, A. Martinewski, A. O. Manzi, A. C. de Araújo, and T. Röckmann (2011), Methane flux, vertical gradient and mixing ratio measurements in a tropical forest, *Atmos. Chem. Phys.*, *11*, 7943–7953.

Randel, W. J., F. Wu, Russell III, J. M., A. Roche, and J. W. Waters (1998), Seasonal cycles and QBO variations in stratospheric CH_4 and H_2O observed in UARS HALOE data, *J. Atmos. Sci.*, *55*, 163–185.

Razavi, A., C. Clerbaux, C. Wespes, L. Clarisse, D. Hurtmans, S. Payan, C. Camy-Peyret, and P. F. Coheur (2009), Characterization of methane retrievals from the IASI space-borne sounder, *Atmos. Chem. Phys.*, *9*, 7889–7899.

Rigby, M., et al. (2008), Renewed growth of atmospheric methane, *Geophys. Res. Lett.*, *35*, L22805, doi:10.1029/2008GL036037.

Schepers, D., et al. (2012), Methane retrievals from Greenhouse Gases Observing Satellite (GOSAT) shortwave infrared measurements: Performance comparison of proxy and physics retrieval algorithms, *J. Geophys. Res.*, *117*, D10307, doi:10.1029/2012JD017549.

Schneising, O., M. Buchwitz, J. P. Burrows, H. Bovensmann, P. Bergamaschi, and W. Peters (2009), Three years of greenhouse gas column-averaged dry air mole fractions retrieved from satellite—Part 2: Methane, *Atmos. Chem. Phys.*, *9*, 443–465.

Shakhova, N., I. Semiletov, A. Salyuk, V. Yusupov, D. Kosmach, and O. Gustafsson (2010), Extensive methane venting to the atmosphere from sediments of the East Siberian Arctic Shelf, *Science*, *327*, 1246–1250.

Shindell, D., et al. (2012), Simultaneously mitigating near-term climate change and improving human health and food security, *Science*, *335*, 183–189.

Spahni, R., et al. (2011), Constraining global methane emissions and uptake by ecosystems, *Biogeosciences*, *8*, 1643–1665.

Spivakovsky, C. M., et al. (2000), Three-dimensional climatological distribution of tropospheric OH: Update and evaluation, *J. Geophys. Res.*, *105*, 8931–8980, doi:10.1029/1999JD901006.

Talagrand, O., and P. Courtier (1987), Variational assimilation of meteorological observations with the adjoint vorticity equation. I Theory, *Q. J. R. Meteorol. Soc.*, *113*, 1311–1328.

Velders, G., (1995), Description of the RIVM 2-dimensional stratosphere model, *RIVM Report 722201002*, Netherlands Participating Organizations, The Netherlands.

Vigano, I. (2010), Aerobic methane production from organic matter, Ph.D. thesis, Faculty of Science, Utrecht University.

Villani, M. G., P. Bergamaschi, M. Krol, J. F. Meirink, and F. Dentener (2010), Inverse modeling of European CH_4 emissions: Sensitivity to the observational network, *Atmos. Chem. Phys.*, *10*, 1249–1267.

Wang, J. S., J. A. Logan, and M. B. McElroy (2004), A 3-D model analysis of the slowdown and interannual variability in the methane growth rate from 1988 to 1997, *Global Biogeochem. Cycles*, *18*, GB3011, doi:10.1029/2003GB002180.

Wecht, K. J., D. J. Jacob, S. C. Wofsy, E. a. Kort, J. R. Worden, S. S. Kulawik, D. K. Henze, M. Kopacz, and V. H. Payne (2012), Validation of TES methane with HIPPO aircraft observations: Implications for inverse modeling of methane sources, *Atmos. Chem. Phys.*, *12*, 1823–1832.

Wofsy, S. C. (2011), HIAPER Pole-to-Pole Observations (HIPPO): Fine-grained, global-scale measurements of climatically important atmospheric gases and aerosols, *Philos. T. R. Soc. A*, *369*, 2073–2086.

Wunch, D., et al. (2010), Calibration of the total carbon column observing network using aircraft profile data, *Atmos. Meas. Tech.*, *3*, 1351–1362.

Xiong, X., C. Barnet, E. Maddy, C. Sweeney, X. Liu, L. Zhou, and M. Goldberg (2008), Characterization and validation of methane products from the Atmospheric Infrared Sounder (AIRS), *J. Geophys. Res.*, *113*, G00A01, doi:10.1029/2007JG000500.

Xiong, X., C. D. Barnet, Q. Zhuang, T. Machida, C. Sweeney, and P. K. Patra (2010), Mid-upper tropospheric methane in the high Northern Hemisphere: Spaceborne observations by AIRS, aircraft measurements, and model simulations, *J. Geophys. Res.*, *115*, D19309, doi:10.1029/2009JD013796.

Yoshida, Y., Y. Ota, N. Eguchi, N. Kikuchi, K. Nobuta, H. Tran, I. Morino, and T. Yokota (2011), Retrieval algorithm for CO_2 and CH_4 column abundances from short-wavelength infrared spectral observations by the Greenhouse gases observing satellite, *Atmos. Meas. Tech.*, *4*, 717–734.